On the statistics of urban heat island intensity

B. Zhou,[1] D. Rybski,[1] and J. P. Kropp[1,2]

Received 12 July 2013; revised 1 October 2013; accepted 3 October 2013; published 17 October 2013.

[1] We perform a systematic study of all cities in Europe to assess the Urban Heat Island (UHI) intensity by means of remotely sensed land surface temperature data. Defining cities as spatial clusters of urban land cover, we investigate the relationships of the UHI intensity, with the cluster size and the temperature of the surroundings. Our results show that in Europe, the UHI intensity in summer has a strong correlation with the cluster size, which can be well fitted by an empirical sigmoid model. Furthermore, we find a novel seasonality of the UHI intensity for individual clusters in the form of hysteresis-like curves. We characterize the shape and identify apparent regional patterns. **Citation:** Zhou, B., D. Rybski, and J. P. Kropp (2013), On the statistics of urban heat island intensity, *Geophys. Res. Lett.*, *40*, 5486–5491, doi:10.1002/2013GL057320.

1. Introduction

[2] The Urban Heat Island (UHI) is a phenomenon, where urban areas experience elevated temperatures relative to the surrounding hinterland [*Oke*, 1987]. Most studies addressing the UHI effect can roughly be categorized into approaches of (i) numerical modeling the physical processes and (ii) empirical analysis, whereas the latter is either based on (a) air temperature records from weather stations or (b) land surface temperatures (LST) from remote sensing.

[3] In the last decades, causative factors of the UHI effect given by *Oke* [1982] have been confirmed and further broadened through a variety of studies around the world. Compared to nonbuilt surroundings, built-up areas of cities differ considerably in albedo, thermal capacity, roughness, etc. which can significantly modify the surface energy budget [*Arnfield*, 2003]. A number of studies suggest that the intensity of UHI could be increased by anthropogenic heating (including contributions from vehicles, building sector, and human metabolism) [*Sailor and Lu*, 2004] as well as CO_2 and pollutants emissions [*McCarthy et al.*, 2010; *Taha*, 1997].

[4] In terms of methodology, physically based numerical models simulate urban energy balance fluxes through the parameterization of urban surface processes (for an overview, we refer to *Masson* [2005]; *Grimmond et al.* [2010]). Empirical approaches, based on either air temperature or LST, attempt to reveal the linkage between the UHI intensity and various descriptive indicators of cities, spanning from biophysical properties (e.g., vegetation, imperviousness) to socioeconomic indices (e.g., population density) [*Holderness et al.*, 2013; *Weng et al.*, 2011]. For a long time, UHI studies suffered from inconsistency and instability with regard to the urban-rural definition, hindering the intercomparison between results. *Schwarz et al.* [2011] compare indicators for quantifying the surface UHI with different urban-rural definitions and report weak correlations among the indicators.

[5] In any case, only individual, few, or up to hundreds of cities have been studied. We overcome this limitation in the number of considered cities by automatically quantifying the effect for all cities in Europe. Therefore, we apply a three-step approach. First, we identify cities in the form of spatial clusters of urban land cover. Second, for each cluster we determine a boundary around the urban cluster of approximately equal area to the cluster area. Third, we calculate LST means of both, cluster and boundary, and define the UHI intensity as the difference between both mean temperatures. Applying this procedure for the entirety of Europe (constrained by the CORINE data, see section 2), we are able to quantify the UHI intensity for ∼130,000 clusters in total from which there are almost 2000 larger than 13 km^2.

[6] We analyze two types of correlations. First, we investigate the UHI intensity of all clusters as a function of the cluster size. We find a characteristic increase with cluster area which we describe by a sigmoid curve. The UHI intensity is seasonally dependent and the saturation is maximal in summer (mean up to 3°C) and considerably smaller in winter. Second, we study the UHI intensity of individual clusters as a function of the boundary temperature. Two findings are striking. On the one hand, not all clusters exhibit increasing UHI intensities with increasing boundary temperatures. For several, the opposite is found, i.e., decreasing cluster temperature with increasing boundary temperature (inverse UHI effect). On the other hand, we find seasonal differences. For the same boundary temperature, different UHI intensities are measured in spring and fall—a pronounced seasonality is found for many clusters, reflecting a characteristic signature and regional heterogeneity due to climate conditions.

2. Data

[7] Our work makes use of two major data sets, (i) land cover information and (ii) land surface temperature (LST).

[8] We base the identification of the urban clusters on the *CORINE land cover* data of the year 2006 at 250 m spatial resolution, covering 38 European Environmental Agency member states and cooperating countries except Greece, with a total area of 5.8 Mkm^2 [*Büttner et al.*, 2007]. The 44 distinguished land use classes are subordinated into five main groups: (a) artificial surface, (b) agricultural areas, (c) forest and semi-natural areas, (d) wetlands, and (e) water

Additional supporting information may be found in the online version of this article.

[1]Potsdam Institute for Climate Impact Research, Potsdam, Germany.
[2]Department of Earth and Environmental Sciences, University of Potsdam, Potsdam, Germany.

Corresponding author: D. Rybski, Potsdam Institute for Climate Impact Research, P.O. Box 60 12 03, 14412 Potsdam, Germany. (ca-dr@rybski.de)

0094-8276/13/10.1002/2013GL057320

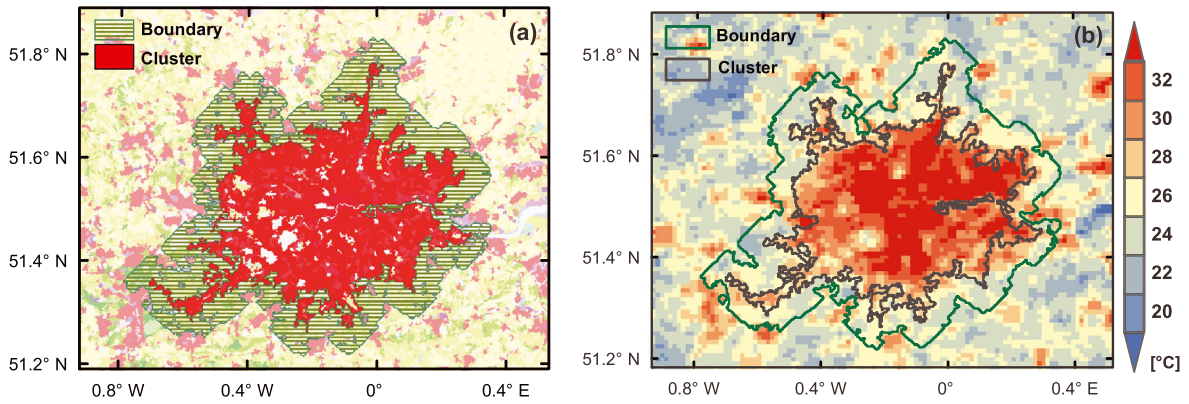

Figure 1. Example of a city cluster and a temperature pattern. (a) Urban cluster identified by CCA (red) and boundary (green hashed) for the Greater London Area with l = 500 m. The urban area of other clusters (pink) are excluded from the identified boundary area. (b) LST for the same area as in Figure 1a captured by the MODIS Aqua at ∼13:30 local time from 2 June 2006 to 9 June 2006. The urban cluster and the urban heat distribution are in agreement.

bodies. Subsequently, the land cover data is reclassified into urban and non-urban ones as described in [*Simon et al.*, 2010], i.e., binary data.

[9] The LST data sets include the MYD11A2 Version 5 data from the Moderate Resolution Imaging Spectroradiometer (MODIS) on the NASA Aqua platform, providing 8 day-mean LST with a spatial resolution of ∼1,000 m, at around 13:30 and 1:30 local time, respectively. We assessed in this paper the LST daytime data from 2006 to 2011. The validation of LST V5 data with in situ measurements indicated that the accuracy of LST data is better than 1°C in most cases [*Wan*, 2008].

3. Method

[10] We define the UHI intensity of a city cluster (labeled with index i), as the difference between the temperature in the cluster and that of the surroundings, i.e., $\Delta T^{(i)} = T_C^{(i)} - T_B^{(i)}$, where $T_C^{(i)}$ and $T_B^{(i)}$ are mean temperatures of the cluster and the boundary, respectively. This definition involves three steps:

[11] 1. Since administrative city boundaries differ from the actual extent, we define cities as clusters of urban land cover. Accordingly, to identify the European cities, we apply the City Clustering Algorithm (CCA) as proposed by *Rozenfeld et al.* [2008] to land cover rather than to population data, since fine-grained population census data are mostly unavailable. CCA involves a clustering parameter l determining up to which distance urban cells are connected with each other, i.e., urban cells within that distance are assigned to the same cluster. We specify $l = 500$ m, i.e., double the resolution of the CORINE data. We denote the cluster size as $S_C^{(i)}$. The highly populated region of Belgium, the so-called Flemish Diamond (Brussels-Antwerp-Ghent-Leuven, see supporting information) becomes the largest urban cluster under this initialization. Paris, the second largest urban agglomeration, is followed by London and Milan.

[12] 2. Analogously, we designate the surroundings of a cluster as the approximate equal-sized boundary area devoid of urban cells of other clusters and sea waters. The boundary is built by consequently forming layers of cell size width around the city cluster (see supporting information for details). Consistently, we denote the boundary size as $S_B^{(i)}$. A similar UHI intensity calculation has been conducted by *Peng et al.* [2012], suggesting minor influence of the boundary size, i.e., 50%, and 100%, 150% of the cluster size.

[13] 3. Since LST data are based on clear-sky conditions, we define a coverage threshold, i.e., the UHI intensity is regarded as valid only if the LST values are available for at least 50 % of the cluster and boundary cells. Moreover, quality control data are supplied with each MODIS pixel, classified into four levels (i.e., $\leq$ 1°C, $\leq$ 2°C, $\leq$ 3°C, $>$ 3°C) which we denote as ϵ. While calculating mean temperatures of clusters and boundaries, we use ϵ for weighting. First, the pixels with a mean LST error $\epsilon > 3$°C are filtered out. Then, the weights are assigned inversely proportional to ϵ^2, i.e., $W = 1/\epsilon^2$. The cluster temperature $T_C^{(i)}$ is therefore a W-weighted arithmetic mean of grid cell temperatures. Analogously, $T_B^{(i)}$ denotes the boundary temperature, considered as a measure for the *background temperature*. Finally, we calculate $\Delta T^{(i)} = T_C^{(i)} - T_B^{(i)}$.

[14] Figure 1a shows an example of a cluster identified by CCA and its boundary for the Greater London Area. As can be seen in Figure 1b, the urban heat pattern mostly matches with the identified cluster, i.e., the city cluster exhibits elevated temperatures. The analogous figure for mean summer temperatures can be found in the supporting information.

4. Analysis

[15] We systematically analyze the UHI intensities, ΔT, for all city clusters identified from the CORINE data by two means, (i) correlations with the cluster size and (ii) correlations with the boundary temperature. In the first case, the ΔT of all clusters are related to the corresponding cluster sizes at *one* observation (ΔT versus S_C for a fixed date), and in the second case, the ΔT of one cluster are related to the corresponding boundary temperatures at *all* available observations (ΔT versus T_B for a fixed cluster).

4.1. UHI Intensity and City Size

[16] It is commonly believed that the UHI effect correlates with cluster size [*Oke*, 1973], but the characteristics of this correlation are poorly understood. Thus, we investigate

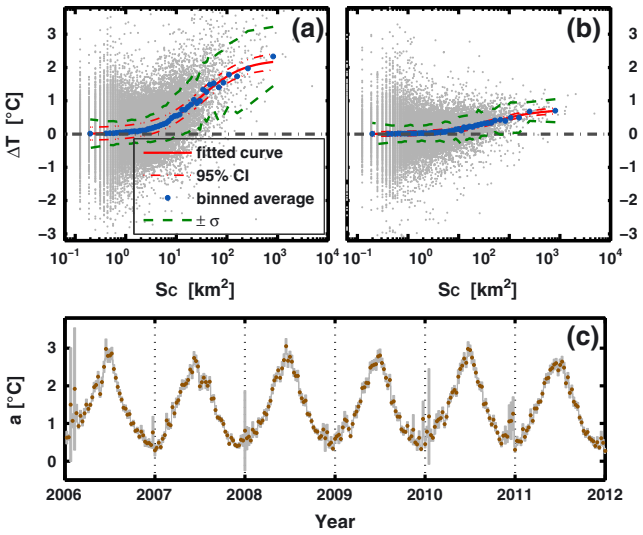

Figure 2. Urban Heat Island intensity as a function of cluster size and seasonal variability. Typical dependence for (a) summer days (4 July 2007 to 11 July 2007) and (b) winter days (2 February 2008 to 9 February 2008) at ∼13:30 local time. Blue dots denote the mean of each bin with the data of individual clusters (grey dots) underlaid. The summer fitting curve exhibits a larger slope and asymptote. 95% confidence intervals of the fitting based on binned data are shown by dashed-dotted lines. The standard deviations σ around the fits are shown by green dashed curves. (c) Time series of the parameter a which the fitting curve saturates at (see equation (1)). The grey bars indicate the 95% confidence intervals, suggesting a naturally larger uncertainty in parameter estimation in winter.

how the UHI intensity depends on cluster size by plotting ΔT as a function of the cluster size for all clusters and two observations in Figures 2a and 2b. Various features can be observed. For large clusters, the typical intensity reaches maximum values of $\sim 2°$C in July (Figure 2a) and $\sim 1°$C in February (Figure 2b). There is considerable spreading of $\sim\pm 2°$C, possibly reflecting local conditions.

[17] In order to characterize the correlations, we perform a binning procedure. Choosing the number of bins and the number of clusters in the first bin (largest clusters), the number of clusters in subsequent lower bins increases exponentially. After identifying the bin limits, the cluster sizes and UHI intensities are averaged in each bin. This binning is motivated by the power-law size distribution of cities [e.g., *Rozenfeld et al.*, 2011]. The binned values in Figures 2(a) and 2(b) suggest a sigmoid relation on a logarithmic scale of cluster size. We employ the empirical function

$$\Delta T = \frac{a}{1 + (S_C/b)^{-c}}\ , \qquad (1)$$

where a is the maximum value at which the fitting curve saturates and b and c determine the inflection and steepness of the curve, respectively. Nonlinear least square optimization is used for fitting equation (1) to the binned values. We find very good agreement between the fitted curves and the empirical values. However, individual city clusters can exhibit UHI intensities considerably above or below the fitting curve. Thus, the fit only characterizes typical behavior.

[18] All parameters are studied time-dependently. In Figure 2c the parameter a, i.e., the saturation value, is plotted versus time for all available observations. The seasonal variability is reflected in the typical saturation UHI intensity with maximum values of up to 3°C in summer (Jun–Aug) and down to 0.5°C in winter (Dec–Feb). The other parameters exhibit seasonal variability as well. In the supporting information, we compare exemplarily LST with 2 m air temperature and find correlations between the temperature records but no correlations between the UHI intensities.

[19] Despite good fitting performance, we need to mention that the analysis does not provide insights into whether there is actual saturation or not, since such a conclusion is restricted by the small number of large cities (as also seen in the power law city size distribution). Nevertheless, it is apparent that the increase of UHI intensity with cluster size decelerates among larger city clusters.

4.2. UHI Intensity and Surrounding Temperature

[20] Since in the previous analysis much information has been averaged out by considering the ensemble of all clusters, next we study individual clusters. We select a cluster and plot the corresponding UHI intensity values of all observations versus the associated boundary temperature, in order to study ΔT given a certain temperature in the surroundings.

[21] Figure 3 displays four examples. Since the raw values of ΔT versus T_B exhibit poor correlations in many cases, we calculate monthly means which are indicated by filled triangles and letters in Figure 3. As can be seen, there are significant seasonal variations. In Paris (Figure 3a), the UHI intensity differs between $\Delta T \approx 3.3°$C in May and $\Delta T \approx 1°$C in September for the same boundary temperature of $T_B \approx 22°$C. A numerical simulation performed by *Georgescu et al.* [2012] reported a maximum UHI intensity during summer for the Arizona Sun Corridor. The UHI was found to be less pronounced during spring and fall, and the least in winter.

[22] In order to better characterize the UHI patterns, we perform a Fourier approximation of both the time series of boundary temperatures, T_B, and UHI intensities, ΔT,

$$F(t) = \sum_{n=1}^{\nu} \left(g_n \cos\frac{2\pi nt}{P} + h_n \sin\frac{2\pi nt}{P} \right) + g_0\ , \qquad (2)$$

where $F(t)$ represents either, T_B or ΔT, $P = 46$, the number of observations for each year, t the times $\{t; t = 1, 2, ...276\}$, g, h, the Fourier coefficients, and specifically g_0 is referred to as the mean of $F(t)$. The order of the analysis, ν, is determined through the Akaike Information Criterion (AIC) [*Akaike*, 1973], which makes tradeoffs between the number of regression parameters and fitting errors. Due to small sample size, we apply an adjusted version by *Sugiura* [1978]. We find that for the majority of clusters, the boundary temperature and the UHI intensity can be well described with the second order Fourier Series ($\nu = 2$) involving five parameters each.

[23] Examples of fitted Fourier curves are given by solid lines in Figure 3. While in Figures 3a and 3b a positive relation can be observed (high UHI intensity coincides with high boundary temperature), in Figures 3c and 3d, the opposite is found (but with smaller amplitude). This inverse UHI effect is also known as the *Oasis Effect* [*Oke*, 1987;

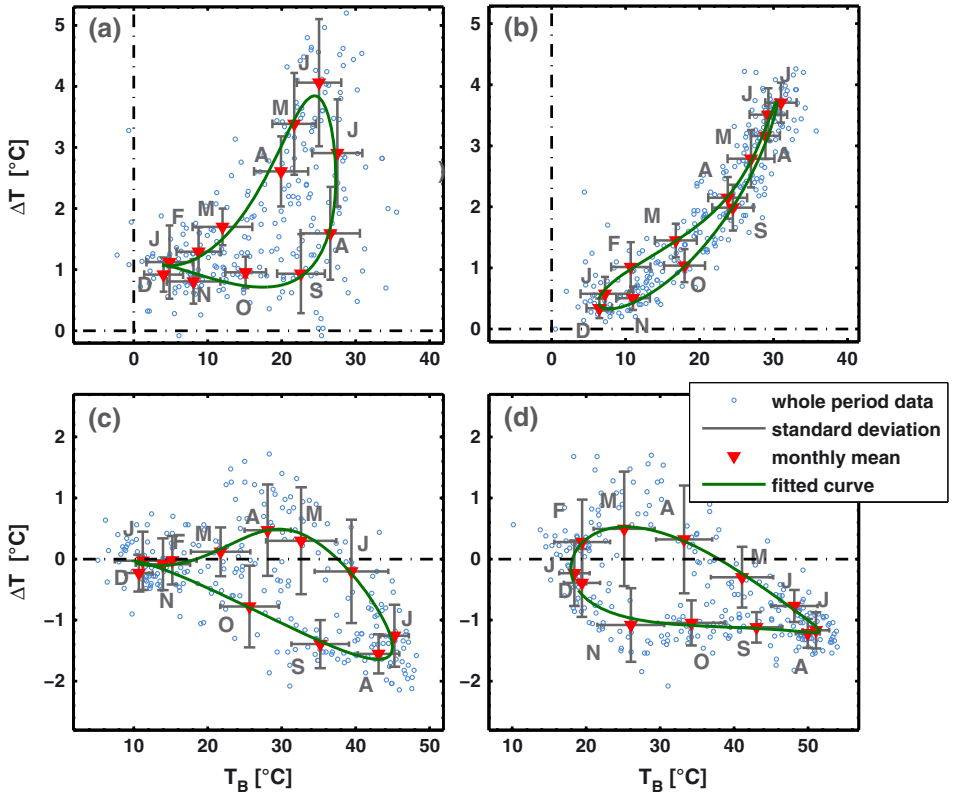

Figure 3. UHI characteristics of individual city clusters. The UHI intensity ΔT is plotted versus the boundary temperature T_B. The values are drawn as small circles, while monthly means are given as red triangles together with the standard deviations (grey error bars). The fitted curves according to equation (2) are plotted as green solid lines. (a) Paris, (b) Milan, (c) Madrid, and (d) Nicosia. The majority of city clusters exhibit a positive correlation between ΔT and T_B and clockwise hysteresis-like curves.

Georgescu et al., 2011; *Brazel et al.*, 2000], being attributed to the arid climate and the interplay with vegetation.

[24] Beyond the positive or negative trend of UHI intensity versus boundary temperature, the hysteresis-like shape of the fitted curve for Paris (Figure 3a) is evident and basically absent in the case of Milan (Figure 3b). As a consequence, in the former, very different UHI intensities can occur given the same boundary temperature, i.e., higher UHI intensities in spring compared to fall. The directionality is always clockwise, in this case with low UHI intensity in winter, higher values in spring, highest in summer, and vanishing intensity in fall. Depending on the location, similar behavior is found for many European city clusters.

[25] The described seasonality in the shape of a hysteresis-like curve represents a phase shift between the UHI intensity and the boundary temperature. We hypothesize that this phenomenon could be due to a differing seasonality in the city and the surroundings, e.g., the temperature in the city follows the astronomical seasons driven by solar radiation and the temperature in the surroundings follows the meteorological seasons corresponding to the regional climate. However, our attempts to trace this claim down to differing vegetation properties of cities with more or less pronounced seasonality were unsuccessful. Another explanation could be phenology, i.e., the different climate in the city and the surroundings could lead to differing onsets of phenological phases so that, e.g., the greening occurs sooner or later.

[26] Last, we want to verify how the UHI patterns are spatially distributed. Therefore, we classify the city clusters according to their hysteresis-like features. We perform the K-means clustering algorithm [*Jain and Dubes*, 1988] on the first harmonics g_0, g_1, and h_1 (six parameters, counting ΔT and T_B separately) of the largest 2000 clusters. Each parameter is normalized before running the K-means clustering, i.e., $X^* = (X - \mu)/\sigma$, where μ is the mean of each parameter and σ is its standard deviation. To obtain an appropriate number of clusters (K), we use the mean silhouette $\bar{s}$ to evaluate the clustering performance as described by *Rousseeuw* [1987]. We run the K-means clustering 200 times with predefined values of K to assess the nondeterministic nature of the algorithm. As can be seen in Figure 4a, for $K = 7$, $\bar{s}$ is relatively large and exhibits the smallest variability, indicating a high clustering stability. City clusters are grouped into the same clusters when they are given the same cluster indices in most of the cases (more than 140 times out of 200 runs).

[27] As can be seen in Figures 4b–4d, the various groups are situated in distinct geographical regions. Group 1 is mostly located in the North-West of Europe, i.e., British Isles and parts of the Atlantic Coasts. Cities of Group 2 are exclusively found in Scandinavia and the Eastern Baltic Coast. While Group 3 consists of Eastern European cities, Group 4 is found in Central Europe. Many large cities are assigned to Group 6, which also covers Central Europe. Groups 5 and 7 are both situated in the Mediterranean regions but

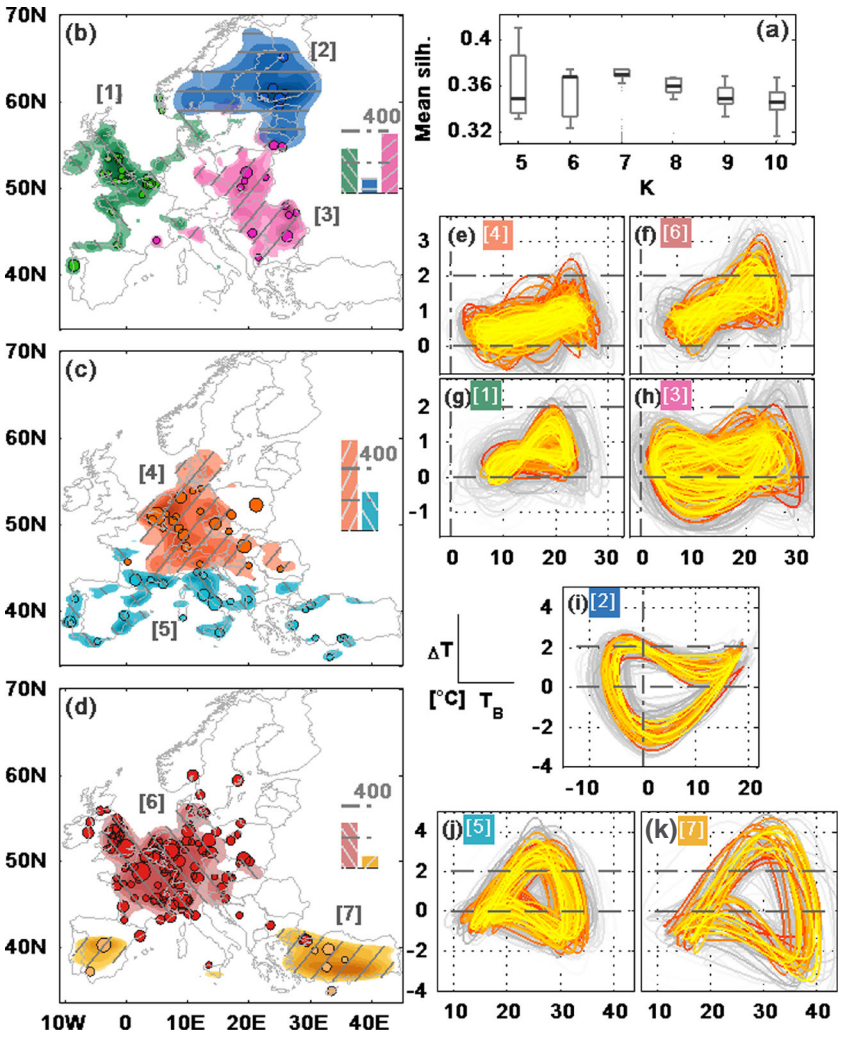

Figure 4. Regional patterns of UHI seasonality. (a) Boxplots of mean silhouette for varying cluster number K (200 runs for each K-value). For $K = 7$, the mean silhouette reaches a local maximum with the lowest variability. (b)–(d) Spatial distribution of the seven groups identified using K-means clustering on the first Fourier coefficients. The largest 200 cities are marked with dots, where the size is proportional to the logarithm of the urban area. The panels include insets displaying the frequency of each group. In general, Groups 1, 3, 4, and 6 are located in the temperate climate zone, whereas Group 2 is in the high latitudes. Groups 5 and 7 are in the Mediterranean climate zone but differentiated into coastal and inland variants. There is an apparent concentration of large cities in Group 6. (e)–(k) Hysteresis-like curves of the respective clusters (as in Figure 3). The clusters, whose data-to-centroid distances are below the 25th percentile, are drawn with colors varying from yellow (closest) to red. The remaining are set to background (grey).

split into coastal and hinterland cities. Each group represents a specific type of UHI seasonality. Groups 1, 3, 4, and 6 are located in the temperate climate zone, which includes the majority of cities. For Group 2, the gentle rises of the curve (see Figure 4i) at both ends could be due to additional household heating in winter and prolonged daylight hours with an increase in absorbed radiation in summer, respectively. Groups 4 and 6 exhibit similar hysteresis-like curves but with different magnitude (Figures 4e and 4f), which is in line with their common geography and the large fraction of big cities in Group 6. Similarly, Groups 5 and 7 differ in their proximity to the coasts but the seasonality is related (Figures 4j and 4k). At water courses, part of the surface energy is converted into latent heat, resulting in lower mean temperatures. Although the grouping is based on the Fourier parameters only, the regional patterns emerge, suggesting that the UHI seasonality is not random, but stems from local climate conditions. Our results are consistent with earlier findings by *Imhoff et al.* [2010] who suggested a clear effect of the ecological setting (biomes) on diurnal and seasonal UHI intensities in the continental USA.

5. Summary

[28] While most studies investigating the UHI intensity are restricted to individual case studies or a limited number of cities, we introduce a statistical approach for the systematic assessment of the UHI effect of all cities and towns in Europe. This analysis is possible because it is entirely based on remote sensing data (land cover and land surface temperature) and the systematic treatment by means of the city clustering algorithm.

[29] We study how the UHI intensity depends on the city cluster size. The empirical values suggest a sigmoid shape and the employed fitting function reaches an asymptotic constant value for large city clusters. In light of ongoing urbanization in many parts of the world, the actual shape of the relation between UHI intensity and city size is of particular interest. Further analyses are necessary to clarify if there is saturation for large city sizes or not. Individual city clusters exhibit intensities considerably above or below the typical size dependence, whereas the spreading is larger in summer. The identification of further explanatory variables of this variability is left for future studies.

[30] The analysis of the UHI intensity depending on the boundary temperature leads to the surprising phenomenon of intra-annual variations of the UHI effect. For many city clusters, the same background temperature comes with very different UHI intensities in spring and in fall. We attribute this phenomenon to the astronomical seasonality of cities and the meteorological seasonality of the surroundings (implying a phase shift). We identify 7 city cluster types which exhibit regional separation. These findings suggest a climatological basis for this new phenomenon. So far, it must be left unanswered but the explanation could be an interesting starting point for future work.

[31] **Acknowledgments.** We thank B.F. Prahl, T. Fluschnik, M. Böttle, S. Schubert, and A. Holsten for useful discussions. We acknowledge the EEA for making available the CORINE land cover data and NASA LP DAAC for the MODIS LST data. The research leading to these results has received funding from the European Community's Seventh Framework Programme under grant agreement 308497 (Project RAMSES).

[32] The Editor thanks Dev Niyogi and an anonymous reviewer for their assistance in evaluating this paper.

References

Akaike, H. (1973), Information theory as an extension of the maximum likelihood principle, in *Second International Symposium on Information Theory,* vol. 19, edited by B. N. Petrov and F. Csaki, pp. 267–281, Akademiai Kiado, Budapest.

Arnfield, A. J. (2003), Two decades of urban climate research: A review of turbulence, exchanges of energy and water, and the urban heat island, *Int. J. Climatol.*, *23*, 1–26, doi:10.1002/joc.859.

Brazel, A., N. Selover, R. Vose, and G. Heisler (2000), The tale of two climates—Baltimore and Phoenix urban LTER sites, *Clim. Res.*, *15*, 123–135, doi:10.3354/cr015123.

Büttner, G., T. Soukup, and A. Sousa (2007), CLC2006 technical guidelines, *Tech. Rep. 17*, Eur. Environ. Agency, Copenhagen.

Georgescu, M., M. Moustaoui, A. Mahalov, and J. Dudhia (2011), An alternative explanation of the semiarid urban area "oasis effect", *J. Geophys. Res.*, *116*, D24113, doi:10.1029/2011JD016720.

Georgescu, M., A. Mahalov, and M. Moustaoui (2012), Seasonal hydroclimatic impacts of Sun Corridor expansion, *Environ. Res. Lett.*, *7*(3), 034026, doi:10.1088/1748-9326/7/3/034026.

Grimmond, C. S. B., et al. (2010), The International Urban Energy Balance Models Comparison Project: First results from phase 1, *J. Appl. Meteorol. Climatol.*, *49*, 1268–1292, doi:10.1175/2010JAMC2354.1.

Holderness, T., S. Barr, R. Dawson, and J. Hall (2013), An evaluation of thermal Earth observation for characterizing urban heatwave event dynamics using the urban heat island intensity metric, *Int. J. Remote Sens.*, *34*, 864–884, doi:10.1080/01431161.2012.714505.

Imhoff, M. L., P. Zhang, R. E. Wolfe, and L. Bounoua (2010), Remote sensing of the urban heat island effect across biomes in the continental USA, *Remote Sens. Environ.*, *114*, 504–513, doi:10.1016/j.rse.2009.10.008.

Jain, A. K., and R. C. Dubes (1988), *Algorithms for Clustering Data*, vol. 355, 320 pp., Prentice Hall, Englewood Cliffs, N. J.

Masson, V. (2005), Urban surface modeling and the meso-scale impact of cities, *Theor. Appl. Climatol.*, *84*(1-3), 35–45, doi:10.1007/s00704-005-0142-3.

McCarthy, M. P., M. J. Best, and R. A. Betts (2010), Climate change in cities due to global warming and urban effects, *Geophys. Res. Lett.*, *37*, L09705, doi:10.1029/2010GL042845.

Oke, T. R. (1973), City size and the urban heat island, *Atmos. Environ.*, *7*, 769–779, doi:10.1016/0004-6981(73)90140-6.

Oke, T. R. (1982), The energetic basis of the urban heat island, *Q. J. R. Meteorol. Soc.*, *108*(455), 1–24, doi:10.1002/qj.49710845502.

Oke, T. R. (1987), *Boundary Layer Climates*, 2nd ed., 435 pp., Routledge, London.

Peng, S., S. Piao, P. Ciais, P. Friedlingstein, C. Ottle, F. M. Bréon, H. J. Nan, L. M. Zhou, and R. B. Myneni (2012), Surface urban heat island across 419 global big cities, *Environ. Sci. Technol.*, *46*(2), 696–703, doi:10.1021/es2030438.

Rousseeuw, P. J. (1987), Silhouettes: A graphical aid to the interpretation and validation of cluster analysis, *J. Comput. Appl. Math.*, *20*, 53–65, doi:10.1016/0377-0427(87)90125-7.

Rozenfeld, H. D., D. Rybski, J. S. Andrade Jr., M. Batty, H. E. Stanley, and H. A. Makse (2008), Laws of population growth, *Proc. Natl. Acad. Sci. U.S.A.*, *105*(48), 18,702–18,707, doi:10.1073/pnas.0807435105.

Rozenfeld, H. D., D. Rybski, X. Gabaix, and H. A. Makse (2011), The area and population of cities: New insights from a different perspective on cities, *Am. Econ. Rev.*, *101*(5), 2205–2225, doi:10.1257/aer.101.5.2205.

Sailor, D. J., and L. Lu (2004), A top-down methodology for developing diurnal and seasonal anthropogenic heating profiles for urban areas, *Atmos. Environ.*, *38*(17), 2737–2748, doi:10.1016/j.atmosenv.2004.01.034.

Schwarz, N., S. Lautenbach, and R. Seppelt (2011), Exploring indicators for quantifying surface urban heat islands of European cities with MODIS land surface temperatures, *Remote Sens. Environ.*, *115*, 3175–3186, doi:10.1016/j.rse.2011.07.003.

Simon, A., J. Fons, R. Milego, and B. Georgi (2010), Urban morphological zones version F2v0: Definition and procedural steps, *Tech. Rep.*, European Topic Centre Land Use and Spatial Information, Eur. Environ. Agency, Barcelona.

Sugiura, N. (1978), Further analysts of the data by Akaike's information criterion and the finite corrections, *Commun. Stat. Theory and Methods*, *7*, 13–26, doi:10.1080/03610927808827599.

Taha, H. (1997), Urban climates and heat islands: Albedo, evapotranspiration, and anthropogenic heat, *Energ. Buildings*, *25*, 99–103, doi:10.1016/S0378-7788(96)00999-1.

Wan, Z. (2008), New refinements and validation of the MODIS Land-Surface Temperature/Emissivity products, *Remote Sens. Environ.*, *112*, 59–74, doi:10.1016/j.rse.2006.06.026.

Weng, Q., U. Rajasekar, and X. Hu (2011), Modeling urban heat islands and their relationship with impervious surface and vegetation abundance by using ASTER images, *IEEE Trans. Geosci. Remote Sens.*, *49*, 4080–4089, doi:10.1109/TGRS.2011.2128874.